Hindawi
International Journal of Antennas and Propagation
Volume 2022, Article ID 7984443, 11 pages
https://doi.org/10.1155/2022/7984443

Research Article

Parameter Estimation of Non-Gaussian Signals for Polarization-Sensitive Augmented Coprime Array: Fourth-Order Cumulant Reduced-Dimensional Capon Algorithm

Meng Yang,[1,2] Haowei Zeng,[1,3] and Xiaofei Zhang[1,3]

[1]*College of Electronic and Information Engineering, Nanjing University of Aeronautics and Astronautics, Nanjing 211106, China*
[2]*Jiangsu Automation Research Institute, Lianyungang 222000, China*
[3]*Key Laboratory of Dynamic Cognitive System of Electromagnetic Spectrum Space (Nanjing University of Aeronautics and Astronautics), Ministry of Industry and Information Technology, Nanjing 211106, China*

Correspondence should be addressed to Haowei Zeng; zenghaowei@nuaa.edu.cn

Received 19 January 2022; Accepted 10 March 2022; Published 27 March 2022

Academic Editor: Xianpeng Wang

In this paper, we investigate the problem of direction of arrival (DOA) and polarization estimation for non-Gaussian signal in polarization-sensitive augmented coprime array. Instead of the second-order cumulant statistics, the fourth-order cumulant statistics of the received signals are used for parameter estimation because they can detect more information of the non-Gaussian signal. First, polarization-sensitive augmented coprime array is designed, where each sensor element is equipped with a pair of orthogonal electric dipoles. Furthermore, a low-complexity reduced-dimensional Capon algorithm which uses the fourth-order cumulant of the received array signal is proposed for DOA and polarization estimation. Only one-dimensional peak search is required by reconstructing peak search function. Theoretical analysis has proven the effectiveness of the algorithm, and simulation results demonstrate that the proposed fourth-order cumulant reduced-dimensional Capon algorithm outperforms the other algorithms.

1. Introduction

The research on directional of arrival (DOA), as a fundamental project in array signal processing, has attracted great attention from relevant scholars all around the world [1, 2]. In recent years, it is proved to be feasible in many fields, such as sonar, radar, and communication system. With the proposal and improvement of related algorithms for different scenarios, the estimate accuracy of DOA is gradually improved, the complexity is also gradually reduced, and more sources could be detected [3–7]. However, existing DOA estimation techniques are usually based on scalar sensor array structures with equal element spacing not greater than half-of-wavelength, which is also called uniform linear array [8]. This array structure can obtain unambiguous DOA estimates while suffering from heavy mutual coupling effects and low system resolution [9]. Simultaneously, only relying on DOA information received by scalar sensor array, it is hard to distinguish different signals impinging on the array from similar directions of arrival. Meanwhile, polarization-sensitive array (PSA) [10] is proposed to obtain another two-dimensional information combined with DOA information, which can distinguish different signals in higher dimensions, especially signals with similar incident angles. Many kinds of polarization-sensitive sensors have been designed for receiving different electromagnetic vector signals, like triad [11], cocentered orthogonal loop and dipole (COLD) [12], and crossed dipoles [13]. Relative algorithms are also proposed for measuring joint DOA and polarization estimates [14–16].

In addition, coprime array (CA) [17, 18] is proposed by extending the array aperture and reducing mutual coupling

effect sparse array, in order to improve the array performance. It solves the problem of compact array structure in uniform linear array, whose phase ambiguity can be eliminated by vectorizing the covariance matrix of the received signal to construct a virtual array. Based on CA, some high-performance DOA estimation algorithms have been proposed in the field of PSA [19, 20]. In [19], the CA is split up into two uniform linear arrays, and a minimum distance parallel factor algorithm is proposed to obtain an accurate estimate, though the advantage of high degrees of freedom (DOF) in CA is not exploited. In order to take full advantage of the large virtual aperture of the CA, a coarray interpolation method is proposed in [20]. However, it suffers from high computational complexity when solving the large stacked recovered covariance matrix.

Augmented CA (ACA) [21], as an improved array, is equipped with more virtual elements than other CAs after vectorization and a closed-form formula in its virtual array's continuous part can be derived, which is more suitable for covariance matrix vectorization. Furthermore, compared with the covariance matrix which only uses second-order statistics of the received signals, fourth-order cumulants can demonstrate more information of non-Gaussian signals [22]. Besides, by constructing the fourth-order cumulants of the received signals, the array aperture of the equivalent virtual array is significantly extended [23], while the noise is suppressed in the fourth-order cumulant due to its Gaussian property [24]. As a result, fourth-order cumulant and its corresponding algorithms have shown great advantages in parameter estimation. However, the CA research on PSA and the corresponding algorithms has just begun, and more and more updated array structure designs and high-precision estimation algorithms are required in this field.

In this paper, we introduce the augmented CA to polarization-sensitive arrays in electromagnetic environment and design a kind of new sparse array called polarization-sensitive ACA (PSACA). Each sensor element is equipped with a pair of orthogonal dipoles, which are orthogonal to each other while the array element location is the same as ACA. On the other hand, a fourth-order cumulant reduced-dimensional Capon (FOC-RD-Capon) algorithm is proposed for non-Gaussian signals. First, the fourth-order cumulant is constructed by received signals, replacing the covariance matrix in traditional Capon algorithm, which can obtain a large amount of consecutive virtual elements. Benefited from the fourth-order cumulant, DOF are increased and virtual array aperture is extended in contrast to the virtual array by vectorization of covariance matrix. Second, considering the high calculation burden of three-dimensional spectral peak search for DOA and polarization estimates, a reduced-dimensional Capon algorithm is proposed, which only requires one-dimensional spectral peak search. The accuracy of the algorithm can be improved by shortening the search interval. The proposed algorithm is proved to have much lower complexity than traditional Capon algorithm. Numerous simulations illustrate the effectiveness of the ACA in polarization-sensitive scenarios and the proposed FOC-RD-Capon algorithm.

To summarize, the contributions of this paper are as follows:

(1) We design the ACA in polarization-sensitive scenario, where each sensor element is a pair of orthogonal dipoles to receive electric field strength vector. Compared with traditional CA, ACA can achieve higher DOF.

(2) We use the fourth-order cumulant signal instead of second-order cumulant signal for non-Gaussian signal, which can demonstrate more information to obtain high estimation performance. Moreover, the equivalent virtual array for the fourth-order cumulant signal has more consecutive elements.

(3) We propose a low-complexity reduced-dimensional algorithm for polarization-sensitive augmented CA, avoiding three-dimensional peak search. Meanwhile, the proposed algorithm enjoys high estimation accuracy with multi-parameter autopairing.

The rest of the paper is arranged as follows.

Section 2 demonstrates the data model of the signal impinging on the PSA. Section 3 introduces the array structure of PSACA and its virtual array element model after employing the fourth-order cumulant. Section 4 elaborates the proposed reduced-dimensional Capon algorithm. Section 5 depicts the simulation results, and Section 6 concludes the paper.

Notations. We use lower-case (upper-case) bold character to imply vector (matrix). $(\cdot)^*$, $(\cdot)^T$, and $(\cdot)^H$ denote the conjugate, transpose, and the conjugate transpose of a matrix or vector, respectively. $\otimes$ denotes the Kronecker product, and $\odot$ represents Khatri–Rao product. $(\cdot)^{-1}$ represents matrix inverse. angle$(\cdot)$ means phase operator. diag$\{\cdot\}$ means diagonalization operator. $\langle a, b\rangle$ means the integer set from a to b, and $E[\cdot]$ means the mathematical expectation of a vector or matrix.

2. Data Model

Consider that K far-field non-Gaussian narrowband signals impinge on the linear array with M sensors where each sensor element consists of a pair of orthogonal electric dipoles to ensure vector receiving capability. The two dipoles with different polarization modes in an element are supposed to be distributed in the direction along with x-axis and y-axis, respectively, which are able to receive the electric component in the corresponding direction. The elevation angles of the signals are $\theta_k \in [-\pi/2, \pi/2]$, $k \in \langle 1, K\rangle$. The corresponding polarization information in the signal can be modeled as two polarization parameters: polarization auxiliary angle $\gamma_k \in [0, \pi/2]$, $k \in \langle 1, K\rangle$ and polarization phase difference $\eta_k \in [-\pi, \pi)$, $k \in \langle 1, K\rangle$. As a result, the single snapshot data model of the received signal on the array is written as [16]

$$\mathbf{y}(t) = [\mathbf{a}_1 \otimes \mathbf{s}_1, \mathbf{a}_2 \otimes \mathbf{s}_2, \ldots, \mathbf{a}_K \otimes \mathbf{s}_K]\mathbf{b}(t) + \mathbf{n}(t), \quad (1)$$

where $\mathbf{a}_k = [e^{j2\pi d_1 \sin\theta_k/\lambda}, e^{j2\pi d_2 \sin\theta_k/\lambda}, \ldots, e^{j2\pi d_M \sin\theta_k/\lambda}]$ denotes the directional vector and $d_m, m \in \langle 1, M\rangle$ is the location of $m-$th sensor element. $\mathbf{b}(t) \in \mathbb{C}^{K\times 1}$ represents the non-Gaussian signal vector while $\mathbf{n}(t) \in \mathbb{C}^{M\times 1}$ is the white Gaussian noise vector. $\mathbf{s}_k \in \mathbb{C}^{2\times 1}$ symbolizes the polarization-space steering vector of $k-$th signal for orthogonal electric dipoles, which can be represented as [13]

$$\begin{aligned}\mathbf{s}_k &= \mathbf{\Phi}(\theta_k)\boldsymbol{\omega}(\gamma_k, \eta_k)\\ &= \begin{bmatrix} 0 & -1 \\ \cos\theta_k & 0 \end{bmatrix}\begin{bmatrix} \sin\gamma_k e^{j\eta_k} \\ \cos\gamma_k \end{bmatrix},\end{aligned} \tag{2}$$

where $\Phi(\theta_k)$ denotes the coordinate matrix only containing DOA information, which is determined by the polarization mode of the electric dipoles, and $\omega(\gamma_k, \eta_k)$ is the polarization vector. Assume that J snapshots are received during a period of time for parameter estimation, and the overall received signal is modeled as [25]

$$\mathbf{Y} = [\mathbf{A} \odot \mathbf{S}]\mathbf{B} + \mathbf{N}, \tag{3}$$

where $\mathbf{A} = [\mathbf{a}_1, \mathbf{a}_2, \ldots, \mathbf{a}_K]$, $\mathbf{S} = [\mathbf{s}_1, \mathbf{s}_2, \ldots, \mathbf{s}_K]$ are the directional matrix and electric matrix, respectively. $\mathbf{B} = [\mathbf{b}_1, \mathbf{b}_2, \ldots, \mathbf{b}_J] \in \mathbb{C}^{K\times J}$ denotes the non-Gaussian signal vector while $\mathbf{N} = [\mathbf{n}_1, \mathbf{n}_2, \ldots, \mathbf{n}_J] \in \mathbb{C}^{2M\times J}$ symbolizes the additive Gaussian noise matrix.

Note that the number of the signals to be estimated in this paper is known. If the number is uncertain, methods such as matrix decomposition [26], information theory [27], or Geist's circle [28] can be used for estimation.

3. ACA and Virtual Elements

Based on the array model in [21], Figure 1 depicts the array structure of the ACA, which is composed of two subarrays. The two subarrays are both uniform linear arrays. Subarray 1, which is marked with white rectangles, is equipped with N array elements with adjacent interval $M\lambda/2$. Meanwhile, subarray 2 is marked with black circles, whose total array elements are $2M$ with adjacent interval $N\lambda/2$. The total element number of the ACA is $2M + N - 1$ because the first element of subarray 1 and subarray 2 is located at the same place. ACA is considered as the improvement of traditional CA because it keeps subarray 1 unchangeable while extending the array aperture of subarray 2 twice as that of CA by equipping $2M$ sensor elements.

It can be obviously concluded from Figure 1 that the sensor element location of each subarray is that

$$\begin{cases} \mathbb{S}_1 = \langle 0, N-1\rangle M\lambda/2, \\ \mathbb{S}_2 = \langle 0, 2M-1\rangle N\lambda/2, \end{cases} \tag{4}$$

where $\langle a, b\rangle$ denotes the integers from a to b. Therefore, the overall position set of the sensor elements is described as $\mathbb{S}_{ACA} = \mathbb{S}_1 \cup \mathbb{S}_2$.

According to the data model for PSA presented in Section 2, the fourth-order cumulant matrix of received signal $\mathbf{Y}$ with J snapshots can be expressed as [24]

$$\begin{aligned}\mathbf{C}_4 = {} & E\left[(\mathbf{Y}\otimes\mathbf{Y}^*)(\mathbf{Y}\otimes\mathbf{Y}^*)^H\right] - E[(\mathbf{Y}\otimes\mathbf{Y}^*)]E\left[(\mathbf{Y}\otimes\mathbf{Y}^*)^H\right] \\ & - E\left[\mathbf{Y}\mathbf{Y}^H\right]\otimes E\left[\left(\mathbf{Y}\mathbf{Y}^H\right)^*\right].\end{aligned} \tag{5}$$

Assume that the signals are independent with each other, and fourth-order cumulant matrix can be considered as the covariance matrix of virtual received signal corresponding to an equivalent virtual array whose element location set is the difference co-array of the physical sensor elements, which can be defined as

$$\mathbb{S}_{ACA\_4} = \left\{d_i - d_j | d_i, d_j \in \mathbb{S}_{ACA}\right\}. \tag{6}$$

Figure 2 demonstrates the virtual array structure after fourth-order cumulant extension for ACA and CA with the same physical sensor elements. There are both 12 physical sensor elements with $M = 4$, $N = 5$ in ACA and $M = 7$, $N = 6$ in CA. As depicted in the figure, CA has 25 consecutive virtual elements while ACA has 47 consecutive virtual elements, which is obviously more than that of CA. Benefited from the merit, ACA can achieve high DOF to detect more signals [29].

4. FOC-RD-Capon Algorithm

4.1. Algorithm Process Introduction. Capon algorithm can obtain multi-parameter estimates simultaneously by a multi-dimensional peak search, which has been widely used in DOA estimation. However, the direct introduction of Capon algorithm from scalar sensor array to polarization-sensitive array will result in the dramatic increase in search dimension, which causes the inevitable high-dimensional search process. To reduce the calculation burden of the Capon algorithm in polarization-sensitive arrays while improving the estimation performance for non-Gaussian signals, a FOC-RD-Capon algorithm is proposed in this section. The introduction will be presented as follows.

Traditional Capon search function for DOA and polarization estimation is expressed as [30]

$$F_{\text{Capon}}\left(a_1, a_2, \cdots, a_Q\right) = \frac{1}{\mathbf{M}^H\mathbf{R}^{-1}\mathbf{M}}, \tag{7}$$

where $\mathbf{R}$ is the covariance matrix of the received signal and $\mathbf{M}$ denotes the array manifold for Q parameters. In PSA scenarios, the array manifold includes three parameters, DOA θ, polarization auxiliary angle γ, and polarization phase difference η, which means three-dimensional peak search is required, but it is unrealistic in engineering application. This part introduces a kind of parameter elimination method for polarization dimensional reduction.

Replacing the covariance matrix by the fourth-order cumulant matrix $\mathbf{C}_4$, define $\mathbf{M} = \mathbf{a}_c(\theta)\otimes\mathbf{s}(\theta, \gamma, \eta)$, where $\mathbf{a}_c(\theta)$ is the directional vector for virtual array structure which is the difference coarray of physical array. Then, the peak search function for PSA fourth-order cumulant scenario is given by

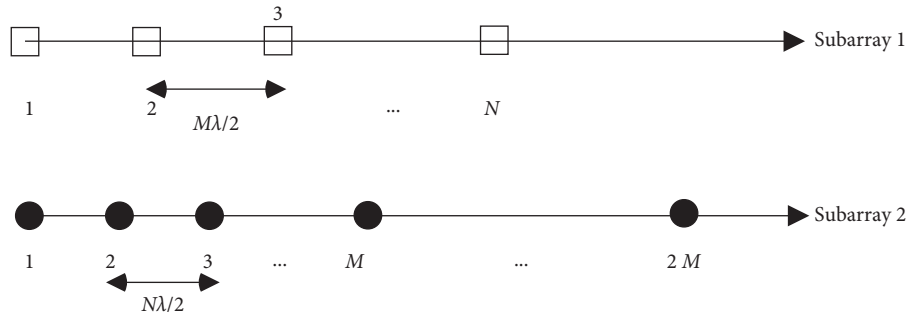

Figure 1: ACA structure.

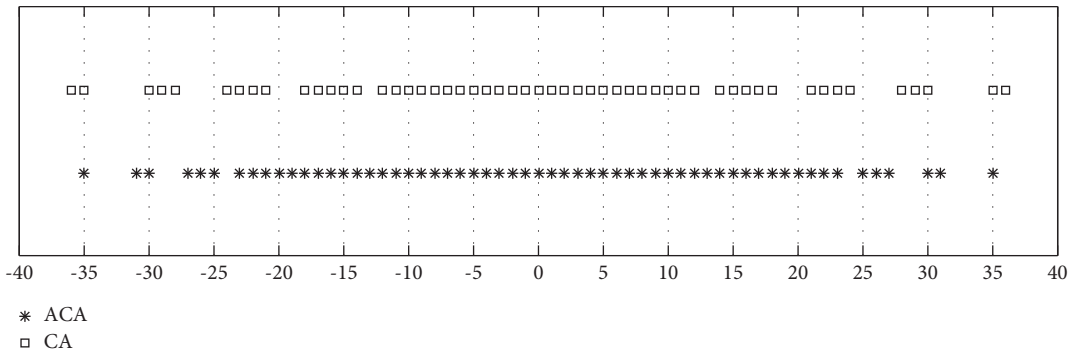

Figure 2: The virtual array structure after fourth-order cumulant extension for ACA and CA.

$$F_{\text{Capon}}(\theta,\gamma,\eta)=\frac{1}{\mathbf{M}(\theta,\gamma,\eta)^H\mathbf{C}_4^{-1}\mathbf{M}(\theta,\gamma,\eta)}. \tag{8}$$

Note that $\mathbf{s}=\Phi(\theta)\omega(\gamma,\eta)$ and a characteristic of Kronecker product is defined as $(\mathbf{AB})\otimes(\mathbf{C}\ \mathbf{D})=(\mathbf{A}\otimes\mathbf{C})(\mathbf{B}\otimes\mathbf{D})$ [25]. The array manifold can be reconstructed as $\mathbf{M}=[\mathbf{a}(\theta)\otimes\Phi(\theta)]\omega(\gamma,\eta)$; therefore, (8) is written as

$$F_{\text{Capon}}(\theta,\gamma,\eta)=\frac{1}{\boldsymbol{\omega}(\gamma,\eta)^H[\mathbf{a}_c(\theta)\otimes\boldsymbol{\Phi}(\theta)]^H\mathbf{C}_4^{-1}[\mathbf{a}_c(\theta)\otimes\boldsymbol{\Phi}(\theta)]\boldsymbol{\omega}(\gamma,\eta)}. \tag{9}$$

Classifying the terms in the function according to the parameters, the terms only about DOA is expressed as $\mathbf{U}(\theta)=[\mathbf{a}_c(\theta)\otimes\Phi(\theta)]^H\mathbf{C}_4^{-1}[\mathbf{a}_c(\theta)\otimes\Phi(\theta)]$. Besides, there is an identity $\omega(\gamma,\eta)^H\omega(\gamma,\eta)=1$ that holds. Then, the peak search function has been transformed into the minimum finding under constraints that

$$F_m(\sigma,\boldsymbol{\omega})=\boldsymbol{\omega}^H\mathbf{U}\boldsymbol{\omega}+\sigma\left(1-\boldsymbol{\omega}^H\boldsymbol{\omega}\right). \tag{10}$$

In order to find the minimum value of (10), we calculate the partial derivative of $F_m(\sigma,\omega)$ about ω^H that

$$\frac{\partial F_m(\sigma,\boldsymbol{\omega})}{\partial\boldsymbol{\omega}^H}=\mathbf{U}\boldsymbol{\omega}-\sigma\boldsymbol{\omega}. \tag{11}$$

Let (11) equal 0 to calculate the final estimates that $\mathbf{U}\omega=\sigma\omega$. Instead of solving the equations, we assume it as the form of eigenvalue and eigenvector pairs, where σ is the eigenvalue and ω is the corresponding eigenvector. Based on the analysis above, the peak search function (9) is expressed as

$$\begin{aligned}F_{\text{Capon}}(\sigma,\boldsymbol{\omega})&=\frac{1}{\boldsymbol{\omega}^H\mathbf{U}\boldsymbol{\omega}}\\&=\frac{1}{\boldsymbol{\omega}^H\sigma\boldsymbol{\omega}}.\end{aligned} \tag{12}$$

Because σ is a constant, (12) is actually the search about the eigenvalue [32].

$$\begin{aligned}F_{\text{Capon}}(\sigma)&=\frac{1}{\sigma\boldsymbol{\omega}^H\boldsymbol{\omega}}\\&=\frac{1}{\sigma_{\mathbf{U},\min}}.\end{aligned} \tag{13}$$

Every peak calculation can be considered as finding the minimum eigenvalue about $\mathbf{U}$ which is only constructed by DOA information. Polarization information is eliminated in Capon search function to tremendously reduce the computational complexity.

After finding K peaks about the DOA estimates $\widehat{\theta}_k, k \in \langle 1, K\rangle$, the corresponding $\mathbf{U}$ is obtained as

$$\mathbf{U}\left(\widehat{\theta}_k\right) = \left[\mathbf{a}_c\left(\widehat{\theta}_k\right) \otimes \mathbf{\Phi}\left(\widehat{\theta}_k\right)\right]^H \mathbf{C}_4^{-1} \left[\mathbf{a}_c\left(\widehat{\theta}_k\right) \otimes \mathbf{\Phi}\left(\widehat{\theta}_k\right)\right]. \quad (14)$$

Polarization matrix $\widehat{\omega}_k$ is measured by the eigen decomposition of $\mathbf{U}(\widehat{\theta}_k)$. Note that $\mathbf{U}(\widehat{\theta}_k) \in \mathbb{C}^{2\times 2}$ has 2 eigenvalue and eigenvector pairs, and the eigenvector whose eigenvalue is the smallest is the estimate $\widehat{\omega}_k$. Ultimately, polarization estimates are obtained as

$$\begin{cases} \widehat{\gamma}_k = \arctan\left(abs\left(\boldsymbol{\omega}_k^{[1]}/\boldsymbol{\omega}_k^{[2]}\right)\right), \\ \widehat{\eta}_k = \text{angle}\left(\boldsymbol{\omega}_k^{[1]}/\boldsymbol{\omega}_k^{[2]}\right), \end{cases} \quad (15)$$

where $k \in \langle 1, K\rangle$ and $\omega^{[i]}$ denotes the $i-$th element in vector ω.

The main steps of the proposed FOC-RD-Capon algorithm are summarized as follows:

Step 1. Compute the fourth-order cumulant matrix of received signal $\mathbf{C}_4$ according to (5).

Step 2. Obtain the peak search function with (8) and reconstruct it according to the characteristic of Kronecker product (9).

Step 3. Establish the search dictionary $\theta_i \in [-\pi/2, \pi/2]$ to calculate $\mathbf{U}(\theta_i)$ with each dictionary element θ_i.

Step 4. Perform eigen decomposition of $\mathbf{U}(\theta_i)$ and find its smallest eigenvalue $\sigma_{\mathbf{U},\min}$.

Step 5. Find K peaks in (13) to estimate $\widehat{\theta}_k$, $k \in \langle 1, K\rangle$.

Step 6. Calculate the eigenvector $\widehat{\omega}_k$ corresponding to the smallest eigenvalue in $\mathbf{U}(\theta_i)$, $k \in \langle 1, K\rangle$.

4.2. Discussion. The calculation burden of the FOC-RD-Capon algorithm mainly results from the following steps. Assume that there are P sensor elements in the ACA. Computing the fourth-order cumulant of the received signal requires $O[J(2P)^4]$. The inverse of fourth-order cumulant matrix needs the complexity of $O[(2P)^6]$. Every peak search consists of $O(64P^2L)$ for L-times peak search. Therefore, it can be summed up that the proposed FOC-RD-Capon algorithm is composed of the complexity of $O(64P^2L + 16JP^4 + 64P^6)$.

Meanwhile, the traditional Capon algorithm without dimensional reduction requires three-dimensional peak search. Computing the fourth-order cumulant and inverse of it requires totally $O[J(2P)^4 + (2P)^6]$, which is the same as the proposed algorithm. However, the three-dimensional peak search needs the complexity of $O(64P^2L^3)$ for L-times search in each dimension. To sum up, the approximate calculation burden of the traditional Capon algorithm is $O(64P^2L^3 + 16JP^4 + 64P^6)$, which is obviously higher than that of the proposed algorithm. Figure 3 shows the comparison of the complexity of the two algorithms with the number of sensor elements.

In addition, ACA is employed for the proposed algorithm due to the following merits:

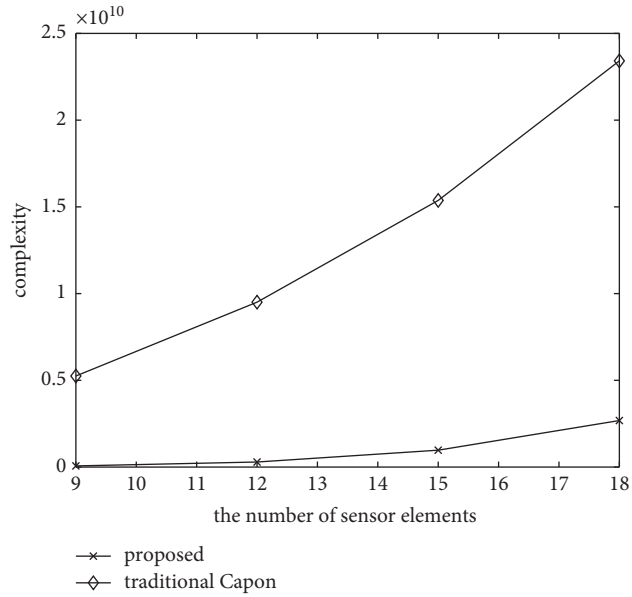

Figure 3: The complexity comparison between the proposed algorithm and the traditional Capon algorithm.

(1) ACA is a kind of sparse array, where array aperture is extended and mutual coupling effect is eliminated. In practice, the coprime numbers M and N can be chosen according to the requirement to satisfy different scenarios. Benefited from the sparse structure, the DOA and polarization estimation results are tremendously improved.

(2) The proposed algorithm uses the fourth-order cumulant statistic instead of the second-order cumulant, where the received signal can be regarded as the signal received by the equivalent virtual array. The virtual array is the difference coarray of physical array. Based on the conclusion and the analysis in Section 3, ACA can achieve more consecutive elements than CA, which means being able to detect more signals.

Cramér–Rao bound (CRB) is often used as the standard error which can be calculated. We derive the CRB formula to evaluate the RMSE performance of the algorithms on the designed ACA. Define $\mathbf{A}_s = \mathbf{A} \odot \mathbf{S}$, $\Pi_{\mathbf{A}_s}^{\perp} = \mathbf{I}_{2P} - \mathbf{A}_s(\mathbf{A}_s^H\mathbf{A}_s)^{-1}\mathbf{A}_s^H$, and $\mathbf{P} = \sum_{j=1}^{J} \mathbf{b}_j\mathbf{b}_j^H/J$, and the formula of CRB for polarization-sensitive ACA is demonstrated as [32]

$$\text{CRB} = \frac{\kappa^2}{2J}\left\{\text{Re}\left[\left(\mathbf{D}^H\Pi_{\mathbf{A}_s}^{\perp}\mathbf{D}\right) \oplus \mathbf{P}^T\right]\right\}^{-1}, \quad (16)$$

where $\mathbf{D} = [\mathbf{d}_1, \ldots, \mathbf{d}_K, \mathbf{e}_1, \ldots, \mathbf{e}_K, \mathbf{f}_1, \ldots, \mathbf{f}_K]$, $\mathbf{d}_k = \partial(\mathbf{a}_k \otimes \mathbf{s}_k)/\partial\theta_k$, $\mathbf{e}_k = \partial(\mathbf{a}_k \otimes \mathbf{s}_k)/\partial\gamma_k = \mathbf{a}_k \otimes \Gamma_k\mathbf{s}_k$, $\Gamma_k = \text{diag}\{\sin\gamma_k, \cos\gamma_k\}$, $\mathbf{f}_k = \partial(\mathbf{a}_k \otimes \mathbf{s}_k)/\partial\eta_k = \mathbf{a}_k \otimes \Xi_k\mathbf{s}_k$, $\Xi_k = \text{diag}\{0, j\eta_k\}$. κ^2 is the power of noise.

5. Simulation Results

Numerous simulations are performed to verify the effectiveness of the designed ACA and proposed FOC-RD-Capon

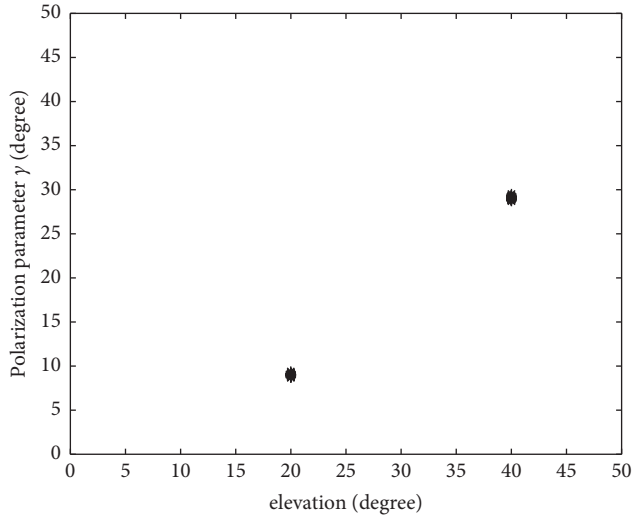

Figure 4: Scatter plot of DOA and polarization parameter γ.

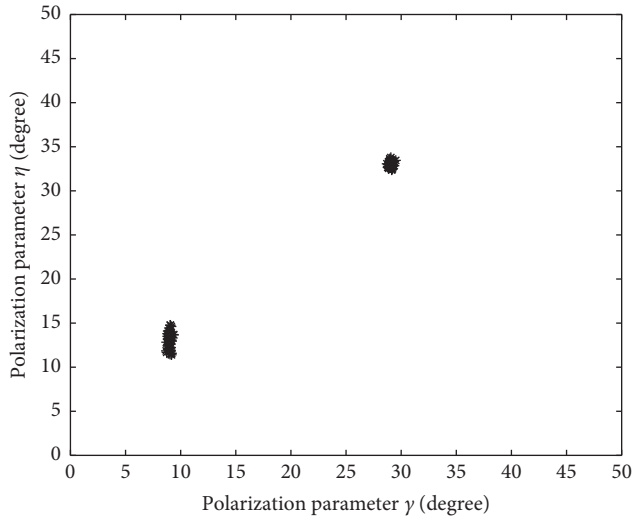

Figure 5: Scatter plot of polarization parameters γ and η.

algorithm, where root mean square error (RMSE) is employed as an evaluation standard to judge the performance. RMSE is defined as

$$\mathrm{RMSE}_a = \frac{1}{K}\sum_{k=1}^{K}\sqrt{\frac{1}{L}\sum_{l=1}^{L}\left[\left(\widehat{a}_{k,l} - a_k\right)^2\right]}, \tag{17}$$

which is the RMSE of parameter a. L denotes the times of independent Monte Carlo simulations. a_k is the actual parameter, and $\widehat{a}_{k,l}$ is its estimate in $l-$th simulation. The two sinusoidal waveform signals are impinging on the ACA, and the DOA and polarization parameters are set as $(\theta_1, \gamma_1, \eta_1) = (20^\circ, 9^\circ, 13^\circ)$, $(\theta_2, \gamma_2, \eta_2) = (40^\circ, 29^\circ, 33^\circ)$. The array structure of ACA is $M = 4, N = 5$, and the total number of physical array elements is 12, which means subarray 1 is equipped with 5 sensor elements and subarray 2 has 8 sensor elements.

5.1. Scatter Plot of the Proposed Algorithm. Figures 4 and 5 depict the scatter plots of DOA and polarization estimates, where 100 independent Monte Carlo simulations are performed. Simulation environments are set as follows: the signal-to-noise ratio (SNR) is 15 dB and the number of snapshots J is 300. As is exhibited in the figures, DOA estimates and two polarization estimates are accurately measured and different parameters are correctly paired. In addition, it can be noticed that the variances of polarization estimates are higher than DOA estimates.

5.2. RMSE Performance of Different Algorithms versus SNR. Figures 6–8 demonstrate the RMSE performance of the proposed FOC-RD-Capon algorithm versus SNR, where CRB curve is given as the standard. Snapshots are fixed as 200 while SNR varies from −10 dB to 20 dB. Compared with the propagator method (PM) [33], estimating signal parameter via rotational invariance techniques (ESPRIT) [34],

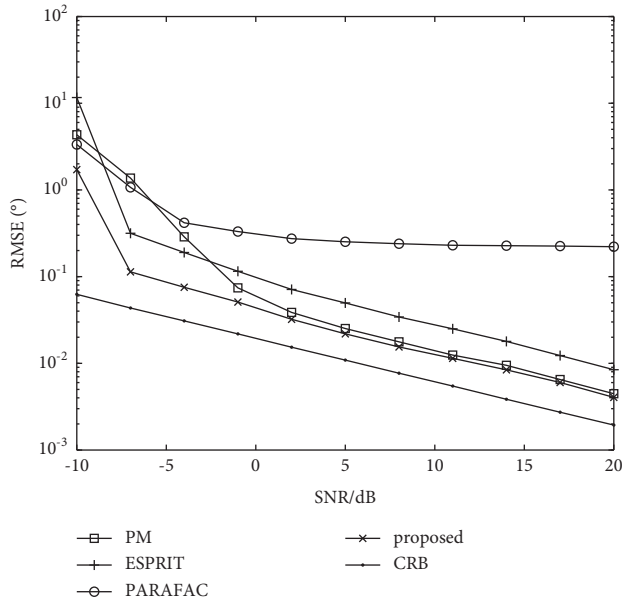

Figure 6: DOA estimation of different algorithms versus SNR.

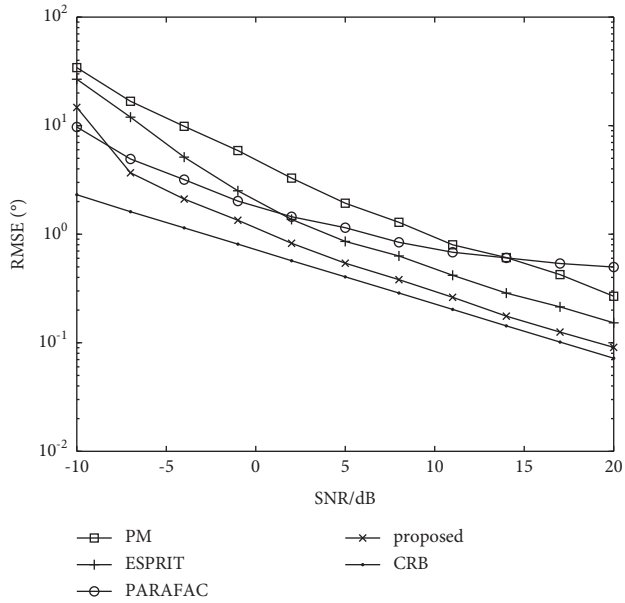

Figure 7: γ estimation of different algorithms versus SNR.

and parallel factor (PARAFAC) [35] algorithms, the proposed algorithm has the lowest RMSE, and its curve is closest to the CRB. Meanwhile, the RMSE of all the four algorithms decreases as the SNR improves, which indicates its influence to the estimates.

5.3. RMSE Performance of Different Algorithms versus Snapshots. Figures 9–11 show the RMSE performance versus snapshots. Similar to Section 5.2, PM, ESPRIT, and PARAFAC algorithms are used for comparison and CRB curve is depicted as the standard. With the increase of

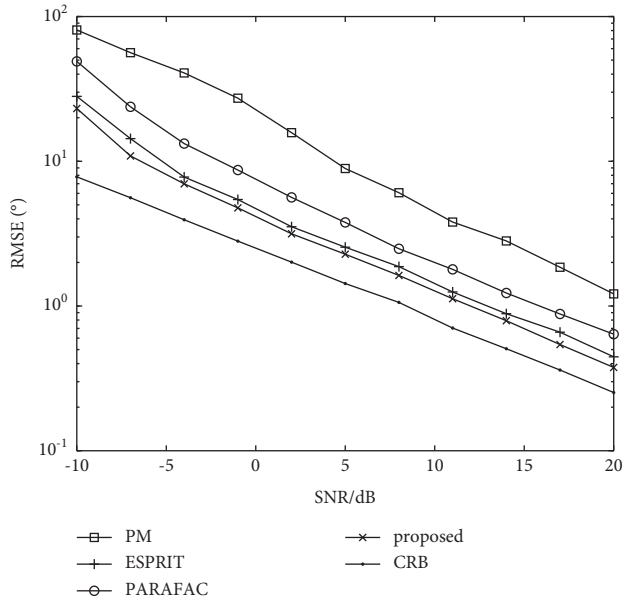

Figure 8: η estimation of different algorithms versus SNR.

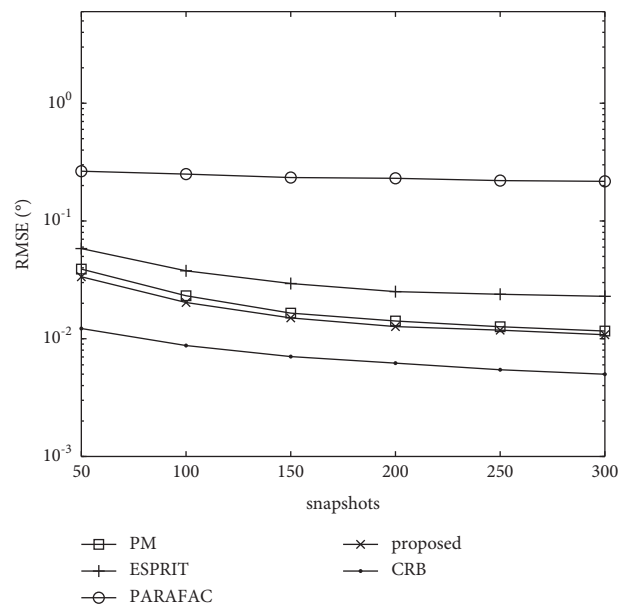

Figure 9: DOA estimation of different algorithms versus snapshot.

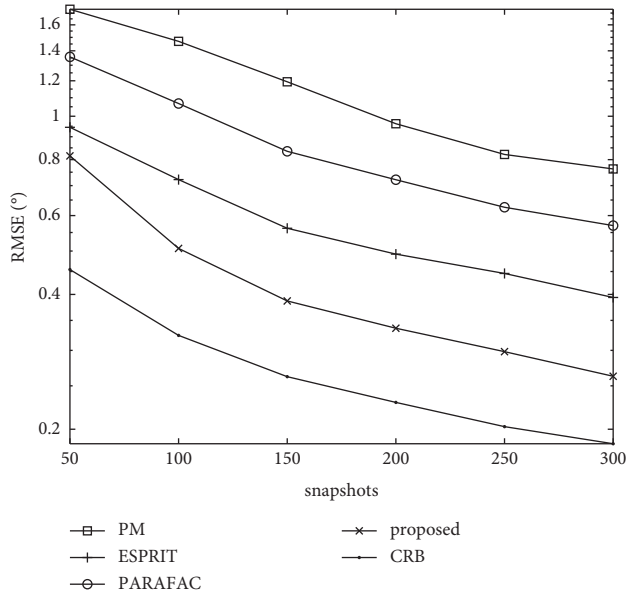

Figure 10: γ estimation of different algorithms versus snapshot.

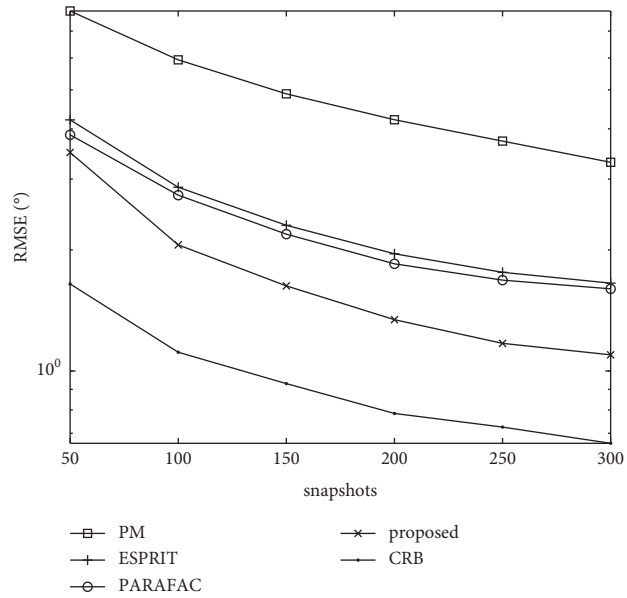

Figure 11: η estimation of different algorithms versus snapshot.

snapshots, the estimation accuracy of all the algorithms is improved. Meanwhile, the proposed FOC-RD-Capon algorithm has the least RMSE whatever snapshots are, which shows its great performance.

6. Conclusion

In this paper, we make use of the inherent information in fourth-order cumulant of non-Gaussian signals, proposing a FOC-RD-Capon algorithm for PSACA. Compared with the scalar sensor arrays, each sensor element of PSASA is equipped with a pair of orthogonal electric dipoles to receive vector signals, which is able to obtain joint DOA and polarization estimates. The proposed algorithm reduces the search dimension of Capon method from three dimensions to one dimension, tremendously reducing the calculation burden. According to the analysis and the numerous simulations, the effectiveness of the proposed FOC-RD-Capon algorithm is confirmed.

Data Availability

The data used to support the findings of this study are available from the corresponding author upon reasonable request.

Conflicts of Interest

The authors declare that they have no conflicts of interest.

Acknowledgments

This study was supported by China NSF (61971217, 61971218, and 61631020), Jiangsu NSF (BK20200444), and National Key Research and Development Project (2020YFB1807602).

References

[1] H. Krim and M. Viberg, "Two decades of array signal processing research: the parametric approach," *IEEE Signal Processing Magazine*, vol. 13, no. 4, pp. 67–94, 1996.

[2] F. Wen, "Computationally efficient DOA estimation algorithm for MIMO radar with imperfect waveforms," *IEEE Communications Letters*, vol. 23, no. 6, pp. 1037–1040, 2019.

[3] X. Zhang, L. Xu, L. Xu, and D. Xu, "Direction of departure (DOD) and direction of arrival (DOA) estimation in MIMO radar with reduced-dimension MUSIC," *IEEE Communications Letters*, vol. 14, no. 12, pp. 1161–1163, 2010.

[4] Z. Yang, L. Xie, and C. Zhang, "Off-Grid direction of arrival estimation using sparse bayesian inference," *IEEE Transactions on Signal Processing*, vol. 61, no. 1, pp. 38–43, 2013.

[5] X. Wu, W.-P. Zhu, and J. Yan, "A toeplitz covariance matrix reconstruction approach for direction-of-arrival estimation," *IEEE Transactions on Vehicular Technology*, vol. 66, no. 9, pp. 8223–8237, 2017.

[6] J. Shi, Z. Yang, and Y. Liu, "On parameter identifiability of diversity-smoothing-based MIMO radar," *IEEE Transactions on Aerospace and Electronic Systems*, to be published, 2021.

[7] J. Cong, X. Wang, C. Yan, L. T. Yang, M. Dong, and K. Ota, "CRB Weighted Source Localization Method Based on Deep Neural Networks in Multi-UAV Network," *IEEE Internet of Things Journal*, 2022.

[8] R. Schmidt, "Multiple emitter location and signal parameter estimation," *IEEE Transactions on Antennas and Propagation*, vol. 34, no. 3, pp. 276–280, 1986.

[9] B. D. Steinberg, *Principles of Aperture and Array System Design: Including Random and Adaptive arrays*, Wiley, Hoboken, NJ, USA, 1976.

[10] J. W. P. Ng and A. Manikas, "Polarisation-sensitive array in blind MIMO CDMA system," *Electronics Letters*, vol. 41, no. 17, pp. 970–972, 2005.

[11] K. T. Wong, "Direction finding/polarization estimation-dipole and/or loop triad(s)," *IEEE Transactions on Aerospace and Electronic Systems*, vol. 37, no. 2, pp. 679–684, 2001.

[12] H. Chen, W. Wang, and W. Liu, "Joint DOA, range, and polarization estimation for rectilinear sources with a COLD array," *IEEE Wireless Communications Letters*, vol. 8, no. 5, pp. 1398–1401, 2019.

[13] X. Zhang, C. Chen, J. Li, and D. Xu, "Blind DOA and polarization estimation for polarization-sensitive array using dimension reduction MUSIC," *Multidimensional Systems and Signal Processing*, vol. 25, no. 1, pp. 67–82, 2014.

[14] B. Hochwald and A. Nehorai, "Polarimetric modeling and parameter estimation with applications to remote sensing," *IEEE Transactions on Signal Processing*, vol. 43, no. 8, pp. 1923–1935, 1995.

[15] M. Hurtado and A. Nehorai, "Polarimetric detection of targets in heavy inhomogeneous clutter," *IEEE Transactions on Signal Processing*, vol. 56, no. 4, pp. 1349–1361, 2008.

[16] B. Zhong and N. Wang, "DOA Estimation Algorithm for Wideband Polarization Sensitive arrays," in *Proceedings of the 2018 2nd IEEE Advanced Information Management, Communicates, Electronic and Automation Control Conference (IMCEC)*, pp. 2516–2520, IEEE, Xi'an, China, May 2018.

[17] C. Zhou, Y. Gu, S. He, and Z. Shi, "A robust and efficient algorithm for coprime array adaptive beamforming," *IEEE Transactions on Vehicular Technology*, vol. 67, no. 2, pp. 1099–1112, 2017.

[18] P. P. Vaidyanathan and P. Pal, "Sparse sensing with Co-prime samplers and arrays," *IEEE Transactions on Signal Processing*, vol. 59, no. 2, pp. 573–586, 2011.

[19] A. Tanveer and X. Zhang, "DOA estimation for coprime EMVS arrays via minimum distance criterion based on PARAFAC analysis," *IET Radar, Sonar & Navigation*, vol. 13, no. 1, pp. 65–73, 2019.

[20] M. Fu, Z. Zheng, W.-Q. Wang, and H. C. So, "Coarray interpolation for DOA estimation using coprime EMVS array," *IEEE Signal Processing Letters*, vol. 28, pp. 548–552, 2021.

[21] K. Zhang, C. Shen, H. Li et al., "Direction of arrival estimation and robust adaptive beamforming with unfolded augmented coprime array," *IEEE Access*, vol. 8, pp. 22314–22323, 2020.

[22] B. Porat and B. Friedlander, "Direction Finding Algorithms Based on High-Order statistics," in *Proceedings of the International Conference on Acoustics, Speech, and Signal Processing*, pp. 2675–2678, IEEE, Albuquerque, NM, USA, April 1990.

[23] F.-G. Yan, X.-W. Yan, J. Shi et al., "MUSIC-like direction of arrival estimation based on virtual array transformation," *Signal Processing*, vol. 139, pp. 156–164, 2017.

[24] M. C. Dogan and J. M. Mendel, "Applications of cumulants to array processing. II. Non-Gaussian noise suppression," *IEEE Transactions on Signal Processing*, vol. 43, no. 7, pp. 1663–1676, 1995.

[25] M. D. Zoltowski and K. T. Wong, "Closed-form eigenstructure-based direction finding using arbitrary but identical subarrays on a sparse uniform Cartesian array grid," *IEEE Transactions on Signal Processing*, vol. 48, no. 8, pp. 2205–2210, 2000.

[26] A. Angzhao Di, "Multiple source location--A matrix decomposition approach," *IEEE Transactions on Acoustics, Speech, & Signal Processing*, vol. 33, no. 5, pp. 1086–1091, 1985.

[27] M. Wax and T. Kailath, "Detection of signals by information theoretic criteria," *IEEE Transactions on Acoustics, Speech, & Signal Processing*, vol. 33, no. 2, pp. 387–392, 1985.

[28] H. T. Hsien-Tsai Wu, J. F. Jar-Ferr Yang, and F. K. Fwu-Kuen Chen, "Source number estimators using transformed Gerschgorin radii," *IEEE Transactions on Signal Processing*, vol. 43, no. 6, pp. 1325–1333, 1995.

[29] P. Pal and P. P. Vaidyanathan, "Coprime sampling and the MUSIC algorithm," in *Proceedings of the Digital Signal Processing and Signal Processing Education Meeting (DSP/SPE)*, pp. 289–294, Sedona, AZ, USA, January 2011.

[30] P. Stoica, P. Handel, and T. Soderstrom, "Study of Capon method for array signal processing," *Circuits, Systems, and Signal Processing*, vol. 14, no. 6, pp. 749–770, 1995.

[31] L. Wang, L. Yang, and G. Wang, "Uni-vector-sensor dimensionality reduction MUSIC algorithm for DOA and polarization estimation," *Mathematical Problems in Engineering*, vol. 2014, no. 21, pp. 682472.1–682472.9, 2014.

[32] P. Stoica and A. Nehorai, "Performance study of conditional and unconditional direction-of-arrival estimation," *IEEE Transactions on Acoustics, Speech, & Signal Processing*, vol. 38, no. 10, pp. 1783–1795, 1990.

[33] S. Marcos, A. Marsal, and M. Benidir, "The propagator method for source bearing estimation," *Signal Processing*, vol. 42, no. 2, pp. 121–138, 1995.

[34] R. Roy, A. Paulraj, and T. Kailath, "ESPRIT--A subspace rotation approach to estimation of parameters of cisoids in noise," *IEEE Transactions on Acoustics, Speech, & Signal Processing*, vol. 34, no. 5, pp. 1340–1342, 1986.

[35] T. D. Pham and J. Möcks, "Beyond principal component analysis: a trilinear decomposition model and least squares estimation," *Psychometrika*, vol. 57, no. 2, pp. 203–215, 1992.